Structural Engineering and Mechanics, *Vol. 75, No. 2 (2020) 229-237*
DOI: https://doi.org/10.12989/sem.2020.75.2.229

Study of a new type of steel slit shear wall with introduced out-of-plane folding

Liusheng He[1,2], Shang Chen[1,2] and Huanjun Jiang*[1,2]

[1]*State Key Laboratory of Disaster Reduction in Civil Engineering, Tongji University, Shanghai 200092, China*
[2]*Department of Disaster Mitigation for Structures, Tongji University, Shanghai 200092, China*

(Received December 12, 2019, Revised February 19, 2020, Accepted February 20, 2020)

Abstract. The steel slit shear wall (SSSW), made by cutting vertical slits in a steel plate, is increasingly used for the seismic protection of building structures. In the domain of thin plate shear walls, the out-of-plane buckling together with the potential fracture developed at slit ends at large lateral deformation may result in degraded shear strength and energy dissipation, which is not desirable in view of seismic design. To address this issue, the present study proposed a new type of SSSW made by intentionally introducing initial out-of-plane folding into the originally flat slitted plate. Quasi-static cyclic tests on three SSSWs with different amplitudes of introduced out-of-plane folding were conducted to study their shear strength, elastic stiffness, energy dissipation capacity and buckling behavior. By introducing proper amplitude of out-of-plane folding into the SSSW fracture at slit ends was eliminated, plumper hysteretic behavior was obtained and there was nearly no strength degradation. A method to estimate the shear strength and elastic stiffness of the new SSSW was also proposed.

Keywords: steel slit shear wall; out-of-plane folding; imperfection; energy dissipation; pinching

1. Introduction

In recent years, the earthquake resilient structure has become a research hotspot in earthquake engineering. Bruneau *et al.* (2003) proposed the concept of earthquake resilience which was the quick recovery of structural function after catastrophic earthquake events. For an earthquake resilient structure, minor/no damage to the main structural system and quick recovery of the function are the two major requirements. To protect the main structural system against earthquakes, energy dissipation devices are usually used. During the past several decades, a large number of energy dissipation devices have been developed, such as viscoelastic dampers, viscous dampers, metallic dampers, tuned mass dampers, earthquake isolation devices, magnetorheological dampers, particle mass dampers etc. Among these devices, metallic dampers are increasingly used because of the low cost, easy manufacturing, stable hysteretic behavior and good reliability, such as X-shaped metal dampers (Tsai *et al.* 1993), shape memory alloy dampers (Wang and Zhu 2017), bucking restrained braces (Takeuchi *et al.* 2012, Shi *et al.* 2018), steel composite dampers (Lee *et al.* 2017, Jiang *et al.* 2019) and steel slit shear walls (SSSWs) (Hitaka and Matsui 2003). Hitaka and Matsui (2003) first proposed the SSSW after the implementation of concrete slit shear wall (Ohmori *et al.* 1966). As it is usually only connected to floor beams through high-strength bolts, after a damaging earthquake, the quick repair of the structure can be achieved by replacing the damaged SSSW. The performance of the steel segments between vertical slits, which are referred as flexural links, is similar to thin columns. Energy is mainly dissipated by the bending deformation of flexural links. They studied the effect of width-to-thickness ratio, aspect ratio, number of slit rows, and edge stiffeners (Hitaka *et al.* 2007). Ke and Chen (2012, 2014) studied the bolt force in connection and the influence of axial force applied in SSSWs. They also proposed a design procedure with energy dissipation considered. To prevent premature out-of-plane bucking in both links and overall plate, different types of out-of-plane constraint were developed, such as using the edge stiffeners (Hitaka *et al.* 2007, Cortes and Liu 2011), backing plate and steel channels (Ma *et al.* 2010), concrete panels (Hitaka *et al.* 2007, Lin *et al.* 2019), and wood panels (Ito *et al.* 2012). Recently, with the primary intention not for energy dissipation, the investigation on the feasibility of using SSSWs for the new function of structural condition assessment was also conducted (Jacobsen *et al.* 2010, Kurata *et al.* 2015, He *et al.* 2015). All the aforementioned research mostly applied relatively thin plate, which inherently involved out-of-plane buckling and accordingly pinched hysteretic behavior. To obtain plump hysteretic curves for good energy dissipation, out-of-plane buckling of both the entire steel plate and individual links are required not to precede the yielding of the flexural links such that the plastic hinges at both ends of the flexural links can be fully developed. The adoption of out-of-plane constraint does improve the hysteretic behavior, which may on the other hand aggravate the tearing at slit ends (Ito *et al.* 2012). For SSSWs without using out-of-plane constraint, the concentrated large plasticity at slit ends also produces material tearing thereby due to the limited ductility of common steel (Cortes and Liu 2011). To have improved material ductility, the material of low-yield-point steel (LYP) with low initial yield strength, large ductility and significant strain hardening had been studied in shear walls (Nakashima *et al.* 1994, Matteis *et al.* 2003, Chen and

*Corresponding author, Professor
E-mail: jhj73@tongji.edu.cn

Copyright © 2020 Techno-Press, Ltd.
http://www.techno-press.com/journals/sem&subpage=7
ISSN: 1225-4568 (Print), 1598-6217 (Online)

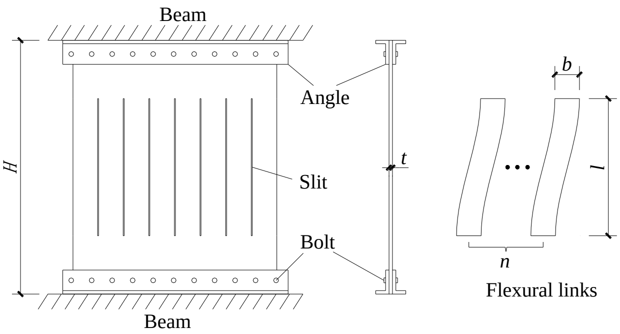

Fig. 1 Steel slit shear wall

Jhang 2006, Zhang *et al.* 2012). LYP SSSWs were investigated to eliminate the fracture at slit ends and further enhance the energy dissipation capacity (He *et al.* 2016), which demonstrated plump hysteretic behavior even without the use of any out-of-plane constraint. However, from the point of view of reducing the cost, it is more desirable to use SSSWs made of common steel.

In this study a new type of SSSWs made of common steel was proposed by intentionally introducing initial out-of-plane folding in the slitted portion. With the addition of initial out-of-plane folding, it is expected to eliminate the fracture at slit ends and enhance its energy dissipation capacity. Three scaled SSSW specimens were designed and tested under reversed cyclic loading. A series of comparative investigations were performed to assess their shear strength, stiffness, energy dissipation, ductility, etc.

2. Strength and stiffness of the SSSW

As shown in Fig. 1, the SSSW is made of a flat steel plate and has a series of rectangular segments (called links) formed by laser-cutting vertical slits. When the wall undergoes in-plane shear deformation, each link between slits behaves as a flexural member and the yielding of links dissipates most of the energy. It is connected only to floor beams, whose interaction with the main lateral-force-resisting system (i.e. columns) is simple and clear.

2.1 Shear strength

Based on the assumption of full plasticity developed at ends of each individual rectangular link, its plastic shear strength Q_{P-Link} is estimated as below:

$$Q_{P-Link} = \frac{2M_P}{l} = \frac{b^2 t}{2l}\sigma_y \tag{1}$$

where $M_P = b^2 t\sigma_y/4$ is the plastic moment of the cross-section; b is the link width; l is the link length; t is the plate thickness; and σ_y is the steel yield strength.

Plastic shear strength of an SSSW with multiple links is estimated by the summation of all individual links as follows

$$Q_P = \sum_{i=1}^{n} \frac{tb^2}{2l}\sigma_y = \frac{ntb^2}{2l}\sigma_y \tag{2}$$

where n is the number of links in one row.

2.2 Elastic stiffness

A rectangular link provides the lateral stiffness as estimated by the following equation (Hitaka and Matsui 2003):

$$K_{link} = \frac{1}{k\dfrac{l^3}{Etb^3} + \dfrac{1.2l}{Gbt}} \tag{3}$$

where E is Young's modulus; G is the shear modulus; 1.2 is the shear deformation shape factor for rectangular section; and $k = (1 + b/l)^3$ is a multiplier that reflects the flexibility at the ends of the flexural links, with $k = 1$ denoting a perfectly rigid boundary and otherwise $k > 1$.

For a slit wall with multiple links, the stiffness can be calculated in a similar way by summing up all individual links. With the contribution of the section without slits through shear deformation considered, the total stiffness of the slit wall can be calculated as follows:

$$K_0 = \frac{1}{\dfrac{1.2(H - ml)}{GBt} + k\dfrac{l^3}{Etb^3}\dfrac{m}{n} + \dfrac{1.2l}{Gbt}\dfrac{m}{n}} \tag{4}$$

where m is the number of rows; n is the number of links in one row; B is the width of the wall; and H is the height of wall. Other geometric notations are defined in Fig. 1.

3. Test program

3.1 Specimen design

A total of three specimens were designed, with detailed dimensions shown in Fig. 2. Specimen 1 was the reference one, which was made by cutting seven vertical slits in a flat steel plate. The slits were made by laser cutting with a numerically controlled machine which was found to be very accurate and efficient. All the links, plate segments separated by vertical slits, had the same width of 72 mm and height of 400 mm. Out-of-plane folding was introduced in the other two specimens. In order to obtain the same link height for all the specimens, the initial link lengths of Specimens 2-3 before introducing the out-of-plane folding were designed as 412 mm and 424 mm, respectively. In the process of manufacturing specimens, the horizontal centerline and top and bottom portions without slits were kept in plane, while the middle slitted portion was pushed carefully out of plane along its one-quarter and three-quarter height lines until the height reached 400 mm. Eventually, the amplitudes of out-of-plane folding were 25mm for Specimen 2 and 35 mm for Specimen 3, respectively. Therefore, Specimen 3 had the largest amplitude of initial out-of-plane folding among the three specimens. The circular holes at two ends of each specimen were set for the connection by high-strength bolts.

The common steel with normal strength was used in specimens. By the test on standard uniaxial tensile coupon specimens, the actual yield strength of the steel was obtained as 346 MPa. The plate thickness was measured as 3.8 mm.

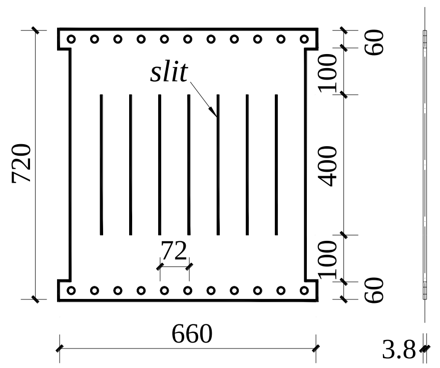

(a) Specimen 1

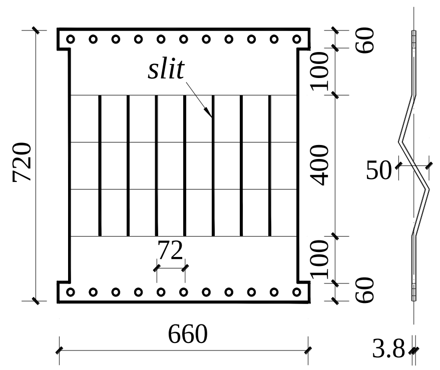

(b) Specimen 2

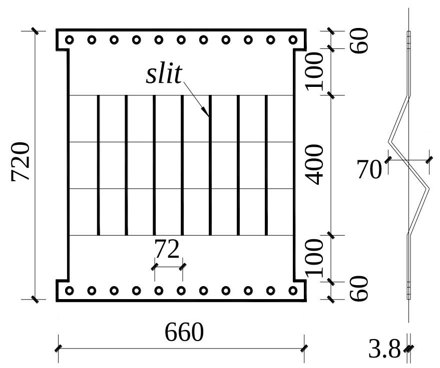

(c) Specimen 3

Fig. 2 Dimensions of test specimens (Unit: mm)

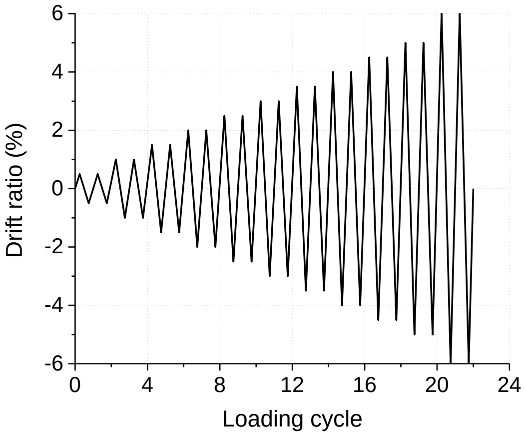

Fig. 3 Incremental two-cycle loading

3.2 Loading protocol

Displacement-controlled cyclic loading was applied at the top of the specimen while the bottom was fixed. Fig. 3 shows the loading protocol. The ordinate of drift ratio is defined as the ratio of lateral deformation to the height of the specimen. For each drift amplitude the specimens were loaded with two cycles. The amplitude increment was 0.5% till the drift ratio of 5%; after that, the maximum amplitude of 6% was used.

3.3 Test setup and instrumentation

The test setup is a portal frame, composed of two top and bottom H-shaped beams, two H-shaped columns and four pins arranged at each corner, as shown in Fig. 4. The height of the portal frame is 1100mm and the spacing between two H-shaped columns is 1960mm. The lateral deformation of the test setup is controlled automatically by using a computer-controlled loading system. The deformation of the load frame is restrained to remain in plane by using out-of-plane restrainers and guiding beams. Two T-shaped beams (250×9/250×14mm) are used to connect the specimen and the load frame by high-strength bolts.

The lateral deformation applied to the SSSW is controlled by the displacement of the jack. The net shear deformation experienced by the SSSW is measured by two displacement transducers, D1 and D2, as shown in Fig. 4(a).

Table 1 Summary of test results

Specimen	Out-of-plane folding (mm)	$Q_{max,t}$ (kN)	$Q_{max,t}$ $/Q_p$	K_t (kN/mm)	K_t/K_0
1	0	52.77	0.79	26.66	0.95
2	25	35.63	0.53	2.89	0.10
3	35	19.60	0.29	1.25	0.04

Note: Q_p is the plastic strength of Specimen 1 according to Eq. (2); K_0 is the elastic stiffness of Specimen 1 according to Eq. (4).

4. Test results and discussions

4.1 Shear strength and elastic stiffness

The maximum shear strength ($Q_{max,t}$) and elastic stiffness (K_t) obtained in the test are listed in Table 1. For

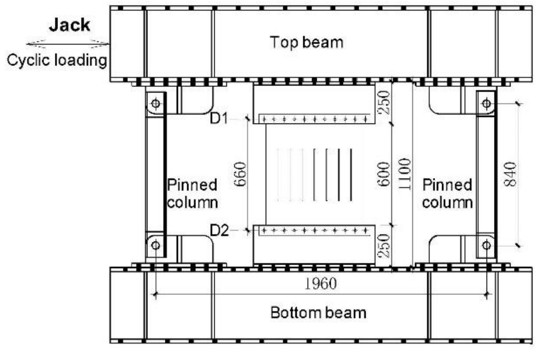

(a) schematic diagram (Unit: mm)

(b) photo in test

Fig. 4 Test setup

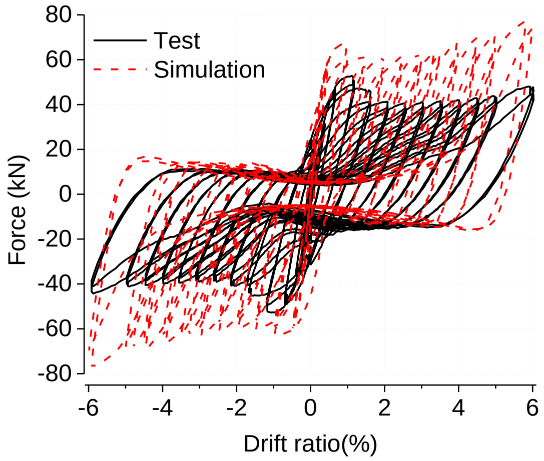

(a) Specimen 1

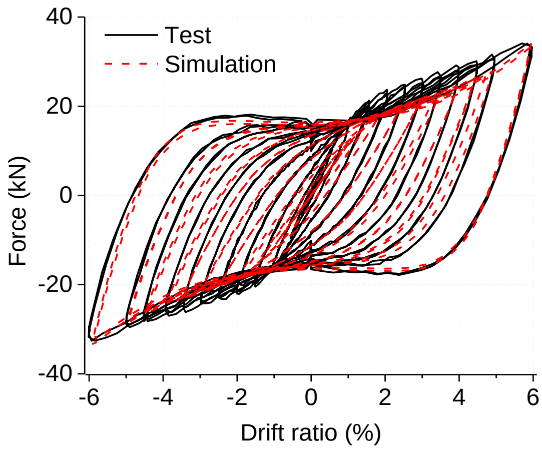

(b) Specimen 2

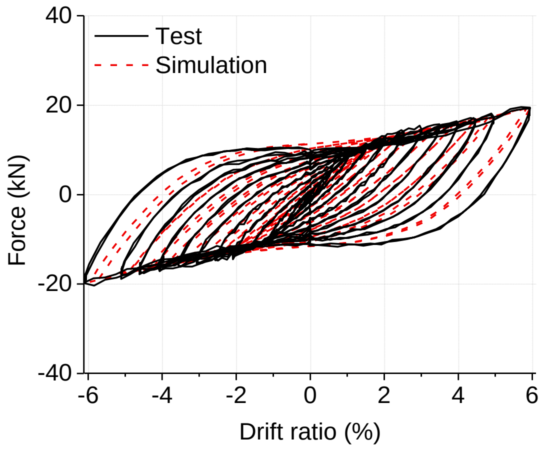

(c) Specimen 3

Fig. 5 Hysteretic curves

Specimen 1 without initial out-of-plane folding, the shear strength and elastic stiffness can be estimated by Eqs. (2) and (4), respectively. The calculated maximum strength is 67.22 kN and elastic stiffness is 28.17 kN/mm. Due to the occurrence of out-of-plane buckling in the links, plasticity did not fully develop at the end sections of links. Therefore, the maximum shear strength obtained in the test was smaller than the predicted value, with a ratio of 79%. The elastic stiffness obtained in the test was quite close to the predicted value, with a ratio of 95%. For Specimens 2-3 with the introduction of initial out-of-plane folding, in principle Eqs. (2) and (4) are no longer applicable. Nevertheless, for comparison purpose, the ratio of their tested shear strength and elastic stiffness to those calculations of Specimen 1 are also listed in Table 1. It can be seen that both the shear strength and elastic stiffness of Specimens 2-3 are much smaller than those of Specimen 1. How to estimate the shear strength and elastic stiffness of SSSWs with initial out-of-plane folding is introduced in a later section.

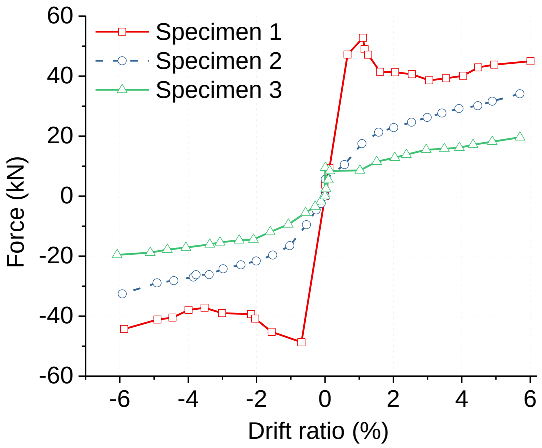

Fig. 6 Skeleton curves

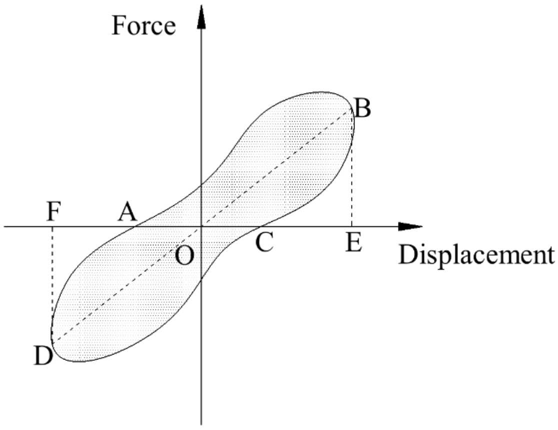

Fig. 7 Estimation of equivalent damping ratio

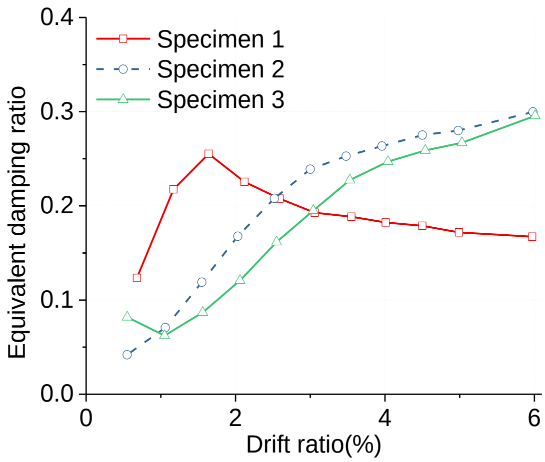

Fig. 8 Equivalent damping ratios

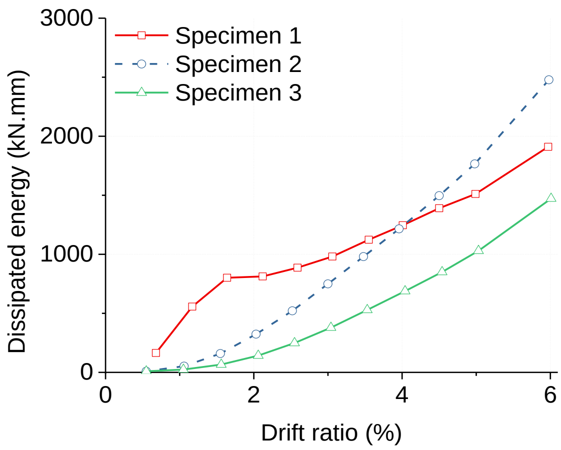

Fig. 9 Comparison of dissipated energy

4.2 Hysteretic behavior and skeleton curve

The hysteretic curve of a structural member can be adopted to comprehensively evaluate its seismic performance from the aspects of ductility, energy dissipation, and strength and stiffness degradation. The hysteretic curves of three specimens are shown in Fig. 5, with the drift ratio being the abscissa and shear force being the ordinate. The pinching effect in the hysteretic curve of Specimen 1 occurred after 1% drift ratio with degradation of energy dissipating capacity, caused by the occurrence of out-of-plane buckling. With the introduction of out-of-plane folding, Specimens 2-3 presented plumper hysteretic behavior.

The load-displacement skeleton curves of three specimens are shown in Fig. 6. For Specimen 1 without initial out-of-plane folding, the strength decreased obviously after notable out-of-plane buckling of links at a drift ratio of 1%, and then it remained stable. For Specimens 2-3 with initial out-of-plane folding, shear strength continued to rise up without obvious peak value. With larger initial out-of-plane folding, the shear strength of Specimen 3 was lower than that of Specimen 2. With the introduction of the initial out-of-plane folding, the shear strength of the specimen decreased. However, with the increase of lateral displacement, the force continued to increase, which was contributed to the tension field effect. Individual links between slits stretched to form the tension field at large displacement. Compared with the common SSSW (for instance, Specimen 1), the presence of initial out-of-plane folding made the tension field effect more obvious. Estimation of the shear strength of SSSWs with initial out-of-plane folding should consider this tension field effect.

4.3 Energy dissipation capacity

The equivalent damping ratio derived from the force-displacement hysteretic curves is often used as an index to judge the energy dissipation efficiency of the member. The larger the equivalent damping ratio of a device, the larger the energy dissipation efficiency is. Adopting the common procedure, the equivalent damping ratio is calculated using the following equation.

$$h_e = \frac{1}{2\pi}\frac{S_{\mathrm{ABC}} + S_{\mathrm{CDA}}}{S_{\mathrm{OBE}} + S_{\mathrm{ODF}}} \tag{5}$$

where $S_{\mathrm{ABC}} + S_{\mathrm{CDA}}$ is the enclosed area of the hysteretic curve and $S_{\mathrm{OBE}} + S_{\mathrm{ODF}}$ is the stored potential energy corresponding to the area of the dash-lined triangles, as shown in Fig. 7.

The equivalent damping ratios of three specimens are shown in Fig. 8, in which loops in the first cycle at each

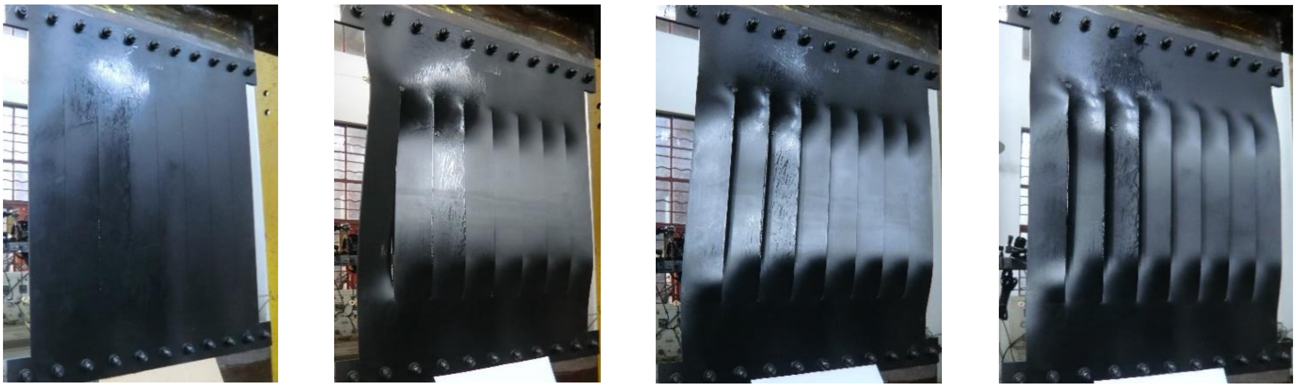

(a) before loading (b) 3% drift ratio (c) 6% drift ratio (d) residual

Fig. 10 Deformed shapes of Specimen 1

drift ratio was used for the calculation. As the lateral displacement amplitude increases, the steel plate links gradually enter plasticity and the dissipated energy gradually increases. Different from Specimen 1, the equivalent damping ratios of Specimens 2-3 kept increasing, while the equivalent damping ratio of Specimen 1 reduced after the drift ratio of 1.6%. From the 2.6% drift ratio, the equivalent damping ratio of Specimen 2 was larger than that of Specimen 1. After the 3.0% drift ratio, the equivalent damping ratio of Specimen 3 was larger than that of Specimen 1. Based on the tested results, it can be concluded that energy dissipation efficiency of SSSWs can be improved by introducing the initial out-of-plane folding, especially at large drift ratios.

To compare the absolute value of energy dissipated, energy dissipation of a single loop at each drift ratio is plotted in Fig. 9. The dissipated energy is the enclosed area of one loop, for instance $S_{\mathrm{ABC}} + S_{\mathrm{CDA}}$ as illustrated in Fig. 7. The second cycle at each drift ratio amplitude was used for the calculation. The amount of energy dissipation for all three specimens continued to increase with the increase of lateral displacement. Within a drift ratio of 4%, the dissipated energy of Specimen 1 was the largest and that of Specimen 3 was the smallest. Beyond that, Specimen 2 began to dissipate the maximum amount of energy. With the introduction of initial out-of-plane folding, the maximum shear strength decreased. However, the energy dissipated was not necessarily small because of the plumpness of the hysteretic curve. Specimen 3 had the largest amplitude of initial out-of-plane folding and thus its energy dissipation was always the smallest. From the perspective of obtaining large shear strength and good energy dissipation, the amplitude of the initial out-of-plane folding should not be too large. Specimen 2, the amplitude of the initial out-of-plane folding about 6% of the link height, seemed to have achieved a good compromise.

Considering practical application, the new SSSW is advised to be installed between floor beams with the aid of additional stiff members, such as inverted V-brace. In this way, the inter-story drift concentrates on the new SSSW. Due to the height difference between the SSSW and story, drift ratio for the SSSW will be amplified and thus relatively large lateral drift ratio for the new SSSW can be realized.

4.4 Observed deformation and damage

The deformed shapes of Specimen 1 at different loading stages are shown in Fig. 10. With the increase of lateral displacement, buckling, in the form of torsional deformation, of rectangular links became obvious. Due to the high stress concentration near the slit ends, micro surface fracture was first observed, followed by the clear steel fracture beyond a drift ratio of 3%. At the completion of 6% drift ratio loading, jack was returned to the initial position. As it can be seen from Fig. 10(d), quite large residual buckling deformation existed.

Figs. 11-12 show the progress of deformed shapes of Specimens 2-3, respectively. Similarly, with the increase of lateral displacement, torsional deformation of individual links became obvious. Compared to Specimen 1 without out-of-plane folding, no notable micro surface fracture was observed, which indicted no high stress concentration at slit ends. Throughout the loading with a maximum drift ratio of 6%, no fracture was observed. After the completion of the drift ratio of 6% loading, both specimens remained intact. It can be concluded that, with the introduction of out-of-plane folding, the potential fracture was eliminated and the overall deformation capacity was largely enhanced.

4.5 Numerical simulation

For Specimens 2-3, the initially introduced out-of-plane folding at the middle slit portions can be deemed as initial imperfection. It is natural to conclude that with the amplitude of initial imperfection increasing both the shear strength and elastic stiffness decrease. However, it is rather difficult to theoretically estimate the shear strength and elastic stiffness for SSSWs with different amplitudes of imperfections. As a compromise, the effect of different amplitudes of initial imperfection can be estimated from a regression analysis of test results together with supplemental numerical simulation.

In the numerical simulation, the commercial finite element code ABAQUS 6.10 was used (Dassault Systèmes 2004), in which a three-dimensional four-node shell element with reduced integration was used to represent the plate. The simple bilinear elastic perfectly plastic material model was used for the steel. In simulating the initial out-

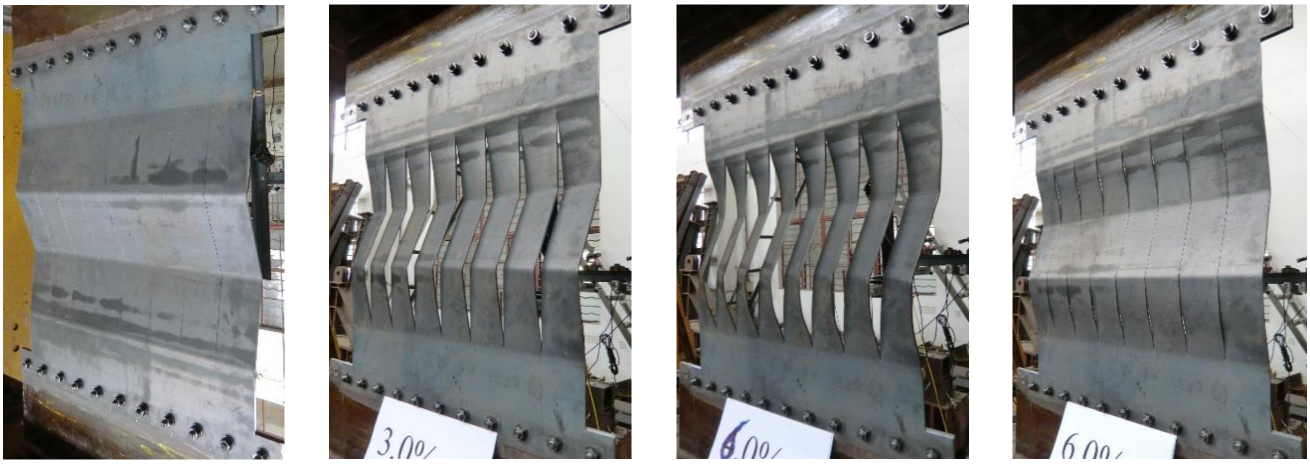

(a) before loading (b) 3% drift ratio (c) 6% drift ratio (d) residual

Fig. 11 Deformed shapes of Specimen 2

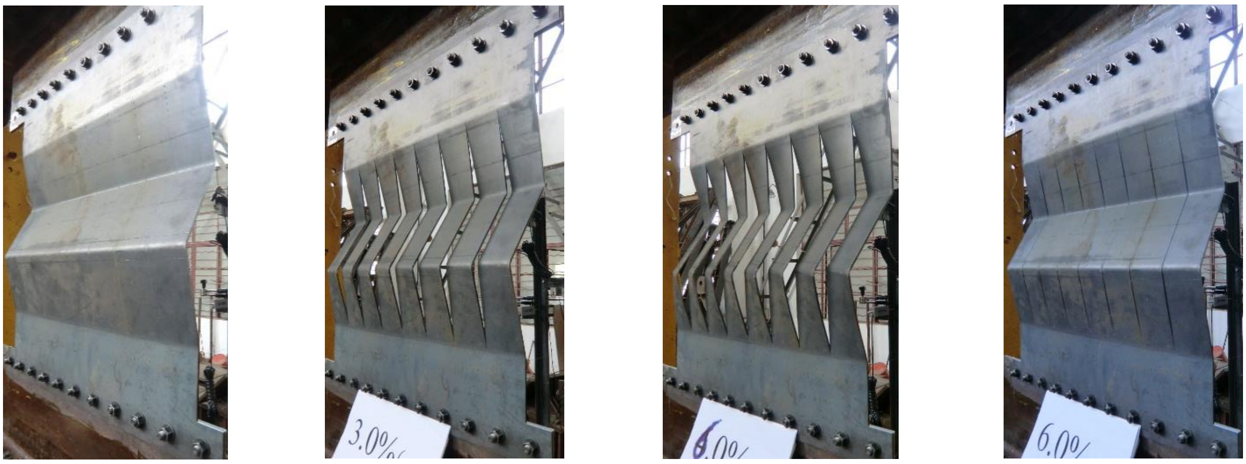

(a) before loading (b) 3% drift ratio (c) 6% drift ratio (d) residual

Fig. 12 Deformed shapes of Specimen 3

of-plane folding, a displacement field associated with the out-of-plane folding was first applied to the numerical model before applying cyclic loading. The numerical model was demonstrated in Fig. 13.

The simulated hysteretic curves of three specimens are also plotted in dashed lines in Fig. 5. The simulation of Specimens 2-3 agreed well with test results, while there was large difference for Specimen 1. Potential reasons for this large difference include: (1) initial imperfection associated with Specimen 1 was rather difficult to quantify than the other two; (2) material defect was unknown; (3) potential occurrence of slippage in the connection; (4) material damage in the form of fracture (only observed in Specimen 1) was not included in the material model. Among these factors, the adopted material model incapable of considering the fracture was the primary reason for the obvious overestimation of shear strength for Specimen 1. Nevertheless, the elastic perfectly plastic material model was still adopted in this study considering its simplicity.

To estimate the maximum shear strength and elastic stiffness of the proposed new SSSW, a parametric study was conducted. A total of 22 SSSWs were modeled (including the tested specimens), with major parameters including three width-to-thickness ratios (defined by b/t, 14.3, 18.8 and 23.8 respectively) and three aspect ratios (defined by l/b, 2.8, 4.2 and 5.6 respectively). The maximum shear strength obtained from both test and simulation was given in Fig. 14. For the shear strength capacity, theoretically the plastic strength Q_P (Eq. (2)), based on the assumption of full plasticity formation at slit ends of SSSWs, should be the upper boundary. However, due to the occurrence of out-of-plane buckling and limited ductility of steel material, the actual tested maximum strength was far below this upper boundary. Therefore, the simulated shear strength larger than Q_P is excluded in the regression analysis of both test and numerical results, which gives Eq. (6) to estimate the maximum shear strength of SSSWs with initial out-of-plane folding.

$$\frac{Q_{max}}{Q_p} = 0.2 + \frac{0.65}{1 + (x/6.5)^6} \tag{6}$$

where x is the normalized out-of-plane folding, defined as the ratio of absolute value of initial out-of-plane folding divided by the plate thickness.

Similarly, the elastic stiffness K of SSSWs with initial out-of-plane folding can be estimated as follows:

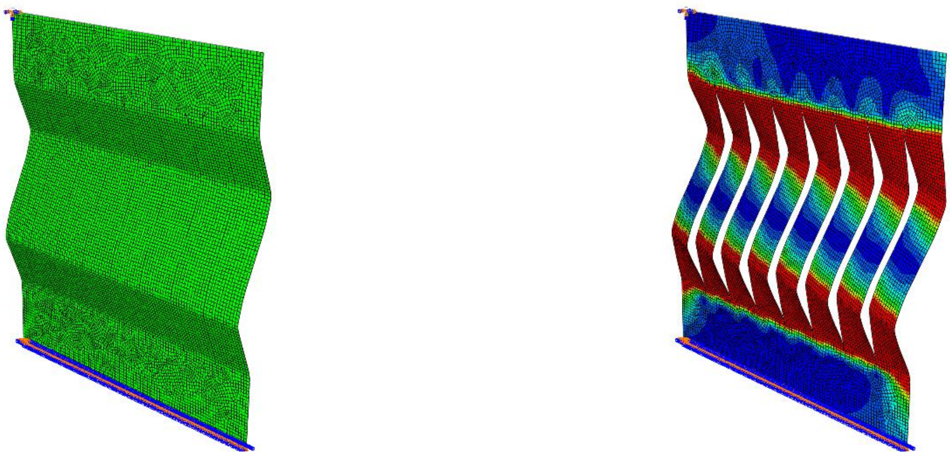

(a) introduced initial out-of-plane folding (b) deformed shape with red color idicating high stress

Fig. 13 Illustration of the numerical model (Specimen 3)

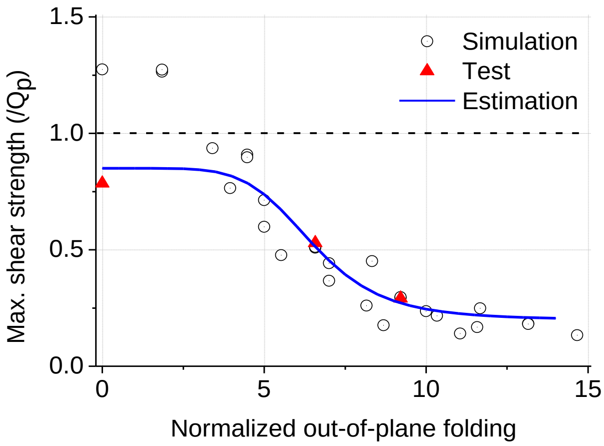

Fig. 14 Proposed estimation of maximum shear strength

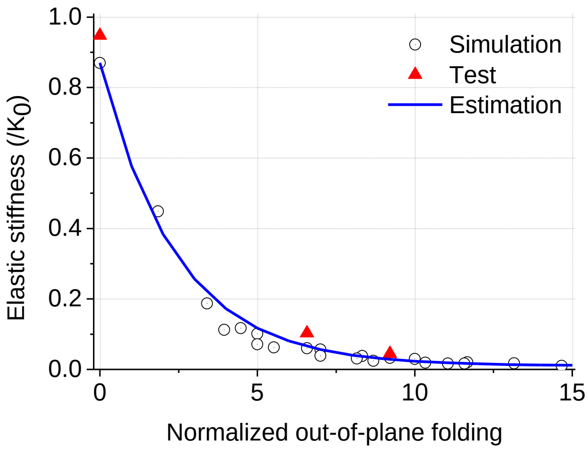

Fig. 15 Proposed estimation of elastic stiffness

$$\frac{K}{K_0} = 0.01 + 0.86\, exp(-\frac{x}{2.4}) \tag{7}$$

In a more intuitive way, Eqs. (6)-(7) are respectively plotted in Figs. 14-15, together with the numerical and test results. The abscissa of normalized out-of-plane folding is the ratio of the absolute value of out-of-plane folding divided by plate thickness. Both the maximum shear strength and the elastic stiffness decrease with the increase of introduced initial out-of-plane folding.

5. Conclusions

The present work studies the effect of introduced out-of-plane folding in SSSWs on their shear strength, lateral stiffness, hysteretic behavior and energy dissipation capacity. Through both experimental and numerical study, major findings are concluded as follows:

- The introduced initial out-of-plane folding decreases both the wall's maximum shear strength and elastic stiffness. However, with the presence of initial out-of-plane folding, the shear strength continues to increase with the increase of lateral displacement and the hysteretic curve is much plumper.
- With the introduction of out-of-plane folding, the potential fracture at slit ends is eliminated and thus the wall's overall deformation capacity is largely enhanced. There is nearly no residual out-of-plane deformation after experiencing even large lateral displacement.
- SSSWs with introduced initial out-of-plane folding have less effect on the lateral stiffness of the main structure. In designing additional damping for seismic protection, the new SSSW could be an effective way for dissipating seismic energy while with little intervention to the main structure.
- A method to estimate both the maximum shear strength and elastic stiffness with consideration of the effect of initial out-of-plane folding is given.
- Future work is required to develop a more refined material model capable of considering the fracture damage at slit ends, to obtain more accurate numerical prediction.

Acknowledgements

The authors are grateful for the support from National Natural Science Foundation of China under Grant No. 51608388 and National Key Research and Development Program of China under Grant No. 2017YFC1500701.

References

Bruneau, M., Chang S.E., Eguchi R.T., Lee, G.C., O'Rourke, T.D., Reinhorn, A.M., Shinozuka, M., Tierney, K., Wallace, W.A., and von Winterfeldt, D. (2003), "A framework to quantitatively assess and enhance the seismic resilience of communities", *Earthq. Spectra*, **19**(4), 733-752. https://doi.org/10.1193/1.1623497.

Chen, S.J., and Jhang, C. (2006), "Cyclic behavior of low yield point steel shear walls", *Thin Walled Struct.*, **44**(7), 730-738. https://doi.org/10.1016/j.tws.2006.08.002.

Cortes, G. and Liu, J. (2011), "Analysis and design of steel slit panel frames (SSPFs) for seismic areas", *Eng. J., AISC*, **48**(1), 1-17.

Dassault Systèmes (2004), ABAQUS Ver. 6.10 User's Manual. http://www.abaqus.com.

He, L., Kurata, M., and Nakashima, M. (2015), "Condition assessment of steel shear walls with tapered links under various loadings", *Earthq. Struct.*, **9**(4), 767-788. https://doi.org/10.12989/eas.2015.9.4.767.

He, L., Togo, T., Hayashi, K., Kurata, M., and Nakashima, M. (2016), "Cyclic Behavior of Multirow Slit Shear Walls Made from Low-Yield-Point Steel", *J. Struct. Eng.*, **142**(11), 04016094. https://doi.org/10.1061/(ASCE)ST.1943-541X.0001569.

Hitaka, T. and Matsui, C. (2003), "Experimental Study on Steel Shear Wall with Slits", *J. Struct. Eng.*, **129**(5), 586-595. https://doi.org/10.1061/(ASCE)0733-9445(2003)129:5(586).

Hitaka, T., Matsui, C. and Sakai, J. (2007), "Cyclic tests on steel and concrete-filled tube frames with Slit Walls", *Earthq. Eng. Struct. Dyn.*, **36**(6): 707-727. https://doi.org/10.1002/eqe.648.

Ito, M., Taniguchi, Y., Tsuboyama, N., Hoki, K. and Nakashima, M. (2012), "Stiffening methods for enhancement of hysteretic performance of slitted steel shear walls", *Proceedings of the 15th World Conference on Earthquake Engineering*, Lisbon, Portugal, September.

Jacobsen, A., Hitaka, T. and Nakashima, M. (2010), "Online test of building frame with slit-wall dampers capable of condition assessment", *J. Constr. Steel Res.*, **66**(11), 1320-1329. https://doi.org/10.1016/j.jcsr.2010.04.011.

Jiang, H., Li, S., and He, L. (2019), "Experimental Study on a New Damper Using Combinations of Viscoelastic Material and Low-Yield-Point Steel Plates", *Front. Mater.*, **6**, 100. https://doi.org/10.3389/fmats.2019.00100.

Ke, K., and Chen, Y. (2012), "Design method of steel plate shear wall with slits considering energy dissipation", *Proceedings of the 15th World Conference on Earthquake Engineering*, Lisbon, Portugal, September.

Ke, K. and Chen, Y. (2014), "Energy-based damage-control design of steel frames with steel slit walls", *Struct. Eng. Mech., Int. J.*, **52**(6), 1157-1176. https://doi.org/10.12989/sem.2014.52.6.1157.

Kurata, M., He, L., and Nakashima, M. (2015), "Steel slit shear walls with double-tapered links capable of condition assessment", *Earthq. Eng. Struct. Dyn.*, **44**(8), 1271-87. https://doi.org/10.1002/eqe.2517.

Lee, J., Kang, H. and Kim, J. (2017), "Seismic performance of steel plate slit-friction hybrid dampers", *J. Constr. Steel Res.*, **136**, 128-139. https://doi.org/10.1016/j.jcsr.2017.05.005.

Lin, X., Wu, K., Skalomenos, K., Lu, L., Zhao, S., (2019), "Development of a buckling-restrained shear panel damper with demountable steel-concrete composite restrainers", *Soil Dyn. Earthq. Eng.*, **118**, 221-230. https://doi.org/10.1016/j.soildyn.2018.12.015.

Ma, X., Borchers, E., Peña, A., Krawinkler, H., and Deierlein G. (2010), "Design and behavior of steel shear plates with openings as energy-dissipating fuses", John A. Blume Earthquake Engineering Center, Stanford University, CA, USA.

Matteis, G.D., Landolfo, R., Mazzolani, F.M. (2003), "Seismic response of MR steel frames with low-yield steel shear panels", *Eng. Struct.*, **25**(2), 155-168. https://doi.org/10.1016/S0141-0296(02)00124-4.

Nakashima, M., Iwai, S., Iwata, M., Takeuchi, T., Konomi, S., Akazawa, T., and Saburi, K. (1994), "Energy dissipation behaviour of shear panels made of low yield steel", *Earthq. Eng. Struct. Dyn.*, **23**(12), 1299-1313. https://doi.org/10.1002/eqe.4290231203.

Ohmori N., Toyama K., Cho T. and Takahashi T. (1966), "Studies on reinforced concrete slit walls", *Summaries of Technical Papers of Annual Meeting AIJ*, **41**, 204 (in Japanese). https://doi.org/10.3130/aijsaxxe.41.0_204.

Shi, Q., Wang, F., Wang, P., and Chen, K. (2018), "Experimental and numerical study of the seismic per-formance of an all-steel assembled Q195 low-yield buckling-restrained brace", *Eng. Struct.*, **176**, 481-499. https://doi.org/10.1016/j.engstruct.2018.09.039.

Takeuchi, T., Hajjar, J.F., Matsui, R., Nishimoto, K., and Aiken, I.D. (2012), "Effect of local buckling core plate restraint in buckling restrained braces", *Eng. Struct.*, **44**, 304-311. https://doi.org/10.1016/j.engstruct.2012.05.026.

Tsai, K.C., Chen, H.W., Hong, C.P., and Su, Y.F. (1993), "Design of steel triangular plate energy absorbers for seismic-resistant construction", *Earthq. Spectra*, **9**(3), 505-528. https://doi.org/10.1193/1.1585727.

Wang, B., and Zhu, S. (2017), "Seismic behavior of self-centering reinforced concrete wall enabled by supere-lastic shape memory alloy bars", *Bull Earthquake Eng.*, **16**, 479-502. https://doi.org/10.1007/s10518-017-0213-8.

Zhang, C., Zhang, Z. and Shi, J. (2012), "Development of high deformation capacity low yield strength steel shear panel damper", *J. Constr. Steel Res.*, **75**, 116-130. https://doi.org/10.1016/j.jcsr.2012.03.014.

PL